EVOLUTION OF SUBGRID SCALE BY PARTICLES IN A TURBULENT CHANNEL FLOW OBTAINED FROM LAGRANGIAN MEASUREMENTS

Yohei SATO
National Institute of Advanced Industrial Science and Technology
Namiki 1-2, Tsukuba Science City, Ibaraki, 305-8564, JAPAN

Anthony D. PARIS
Thermosciences Division, Department of Mechanical Engineering
Stanford University
Stanford, California 94305, U.S.A.

Tomohiko TANAKA and Koichi HISHIDA
Department of System Design Engineering, Faculty of Science and Technology
Keio University
3-14-1 Hiyoshi, Kohoku-ku, Yokohama, 223-8522, JAPAN

Evolution of subgrid scale (SGS) stresses by particles in a fully-developed channel flow was investigated by Lagrangian measurement technique. Digital particle image velocimetry and a high-speed CCD camera mounted on a shuttle moving with particle mean streamwise velocity were used to simultaneously detect particle and fluid information amongst particles. Directional interactions between particles and turbulence were ensured by examinations of the real SGS stresses seen by particle. Turbulence augmentation by particles greater than the Kolmogorov micro scale was induced by regions of the energy backscatter on both sides of particles, which means that particles enhance energy transport from subgrid scales to grid scales. An increase in particle volumetric fraction enhances both the SGS energy dissipation and the amount of energy backscatter control.

INTRODUCTION

One of the most important aspects of dispersed two-phase flows is the interactions of solid particles or liquid droplets with turbulent flow fields. In fact the performance of many engineering devices as well as natural processes encompass dispersed two-phase flows. An increased understanding of the fundamental phenomena that drive the complex interactions between the particle cloud and turbulent carrier flow is needed to ultimately improve the design of engineering devices in which these flows occur. The available experimental data show that the addition of small particles suppresses turbulent kinetic energy, while large particles increase turbulence (Tsuji and Morikawa 1982, Tsuji *et al.* 1984, Fleckhause *et al.* 1987, Rogers and Eaton 1991, Kulick *et al.* 1994). While the works using direct numerical simulation by Squires and Eaton (1990), Elghobashi and Truesdell (1993), and Boivin *et al.* (1998) have advanced our understanding, the effect of particles on turbulence modification is not fully resolved up to this day.

To date the macro-analyses present the following consensus interpretation. Gore and Crowe (1989*a*, 1989*b*) compiled data, foremost expressing the ratio of particle diameter to a characteristic length scale of the turbulence as a key parameter. They suggested that the critical value of the ratio separating regions of attenuation and augmentation was on the order of 0.1. Eaton (1994) reviewed past experiments and simulations in turbulence modification of simple flows and showed significant turbulence attenuation for mass loading ratios greater than 0.1. Sato and Hishida (1996) introduced the multiple-time-scale concept to more accurately model the energy transport due to particles from the production range to the transfer range. An outcome of these works revealed that the particle size and loading have a significant influence on turbulence modification.

The objective of this study is to investigate energy transport by particles in a turbulent channel flow via Lagrangian measurement (Sato *et al.* 1997, 2000). Evolution of subgrid scale (SGS) stresses amongst particles was first examined using filtered velocity *seen by particle*. Sato *et al.* (2000) found the directional structure of turbulence augmentation by particles, however, they investigated the particle/turbulence interactions in only streamwise (X) and transverse (Y) directions. The present study was performed in both X-Y and X-Z (spanwise) planes in order to give further insight into development of SGS model for dispersed two-phase turbulent flows. None of the effective SGS models and universal understanding for energy transport by particles existed in the literature, therefore the efforts obtained from the present experiments will make significant contribution to resolve the directional scale-dependent structure in multiphase flows.

EXPERIMENTAL SETUP

Experimental facility

The present experiments were performed in a two-dimensional, vertical channel with downflow of water, identical to that of Sato *et al.* (1997, 2000). The channel was vertically oriented so that the gravitational force on the particles was aligned with the direction of flow. Boundary-layer trips

Table 1. Particle properties

Properties			glass	glass
number mean diameter	d_p	[μm]	396.4	396.4
stan. dev. of diameter	σ_p	[μm]	32.3	32.3
density	ρ_p	[kg/m^3]	2,590	2,590
terminal velocity	V_t	[mm/s]	102	102
particle time constant	τ_p	[ms]	10.4	10.4
particle Reynolds number‡	Re_p		50.0	50.0
particle mass loading ratio	ϕ_{mass}		3.3×10^{-4}	8.6×10^{-4}
particle volumetric fraction	ϕ_{vol}		1.8×10^{-4}	3.3×10^{-4}

‡mean value calculated using instantaneous particle Reynolds number

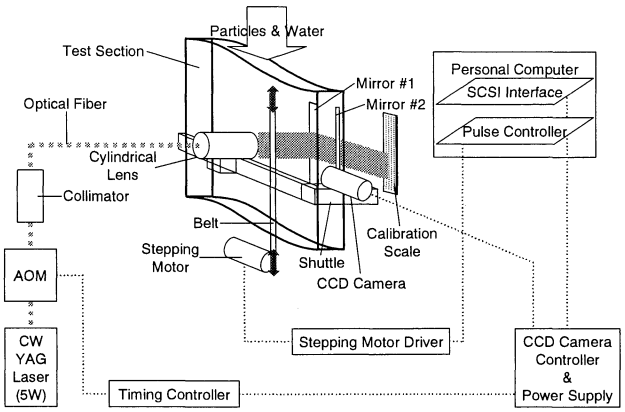

Figure 1. Schematic of digital particle image velocimetry and vertical water channel.

were affixed to both walls at the entrance of a 1.0 m long, 30×250 mm test section. All the experiments were run at a centerline mean velocity of 155 mm/s, corresponding to a Reynolds number of 5,740 based on channel width. The temperature of water was kept constant by using a heater to avoid varying fluid properties. The Kolmogorov micro length scale, η, at the channel centerline was 252 μm which was calculated by direct measurements of dissipation rate of turbulent kinetic energy.

Glass particles were used in the present set of experiments and their characteristics are compiled in table 1. The particle size was chosen with the following strategy: (i) smaller than the energy-containing scales of the flow and (ii) slightly greater than the Kolmogorov micro scale of turbulence. The particle size distributions were determined by using successively smaller sieves, while the particle sphericity was checked using a microscope.

Experimental techniques

Velocities of both phases were obtained by using a digital particle image velocimetry (DPIV) developed by Sakakibara *et al.* (1993) and Sato *et al.* (1997, 2000). Figure 1 shows a schematic illustration of the DPIV. Velocities were calculated by a cross-correlation technique between two images. Polyethylene particles of 5 μm (density of 960 kg/m^3) were added as a tracer to the liquid phase. The thickness of the YAG-laser light sheet was 3.0 mm in the test section.

A high speed CCD camera (KODAK Motion Corder Analyzer SR-500) and a cylindrical lens

(*a*)

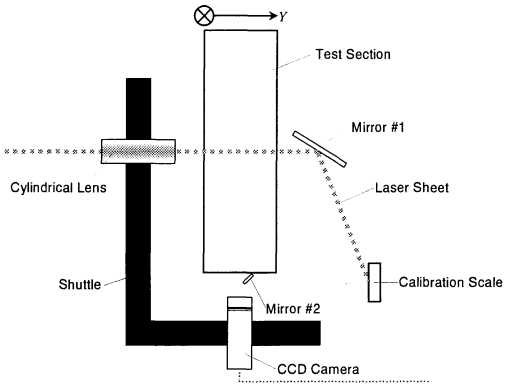

(*b*)

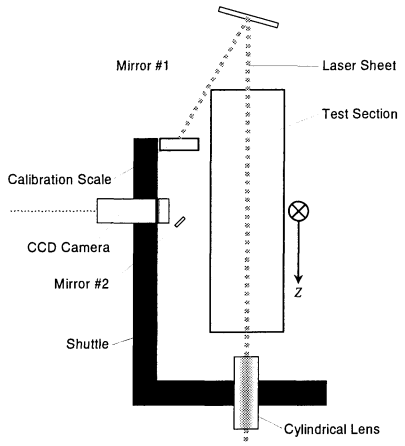

Figure 2. Top view of experimental facility for measurement in (*a*) *X-Y* plane and (*b*) *X-Z* plane.

were mounted on a moving shuttle in order to establish the Lagrangian measurement technique. The present measurement system simultaneously detected particles and fluid information. The shuttle moved from top to bottom, parallel to the water channel with mean streamwise velocity of the focused particles. A stepping motor was used to control the shuttle's velocity and it is necessary to calibrate influence of vibration of shuttle on its velocity. A special calibration scale in which solid marks were randomly distributed as if particle concentration were detected, as shown in figure 1, was added to the present system (Sato *et al.* 1997, 2000). The CCD camera captured the images of flow field in the test section and the calibration scale by using mirror 2, illuminated by a laser sheet via mirror 1. Figure 2 illustrates top view of moving shuttle. Measurements in *X-Z* plane was

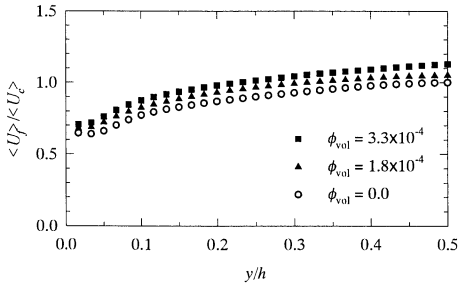

Figure 3. Profiles of mean streamwise velocity of water in the presence of particles.

established after the location of the CCD camera was exchanged for the optical system. By using the DPIV system combined with the moving shuttle it is possible to calibrate the shuttle's vibration per unit image. The measurement uncertainty in these experiments due to the velocity calibration was 2.0% for instantaneous velocity measurements. The particles and surrounding fluid were measured by the high-speed CCD camera in a matter of few seconds. Subsequently velocities in time series were calculated within an interval of 1/125 s (= 8 ms).

RESULTS AND DISCUSSION

Properties of the Eulerian field

Figure 3 shows profiles of the mean streamwise velocity in the presence of particles. The coordinate of the figure has nondimensionalized values based on the centerline mean velocity in single phase, $\langle U_c \rangle$, of 155 m/s and a channel width, h, of 30 mm. It is observed that the particle-laden mean fluid velocity was significantly accelerated at ϕ_{vol} = 3.3×10^{-4}.

Further insight into the nature of turbulence augmentation by particles is provided by the flow power spectra in all the directions. Figure 4 shows profiles of streamwise velocity power spectra of water at the centerline of the channel in the presence of glass particles. The ordinate is normalized by kinematic viscosity of water, ν, and dissipation rate of turbulent kinetic energy of water, ε, in single phase, while the abscissa is normalized by the Kolmogorov micro length scale of water, η, in single phase. An increase in turbulence energy in the low-wave-number region was observed with increasing values of particle volumetric fraction, which is identical to the conclusions obtained by Sato and Hishida (1996). A significant increase was observed in the transverse direction, as shown in figure 5. It can be concluded that the directional interactions between fluid turbulence and particles occurred as reported by Hishida and Sato (1999) and Sato *et al.* (2000).

Basic statistics of SGS stresses

The filtered velocity field is formally defined as

$$\tilde{u}_{f_i}(x,y) = \int_{-\infty}^{\infty}\int_{-\infty}^{\infty} U_{f_i}(x',y')G(x-x',y-y')\mathrm{d}x'\,\mathrm{d}y' \quad (i=1,2), \quad (1)$$

where $G(x,y)$ is a spatial low-pass filter with characteristic width Δ. The filters used in the present study are

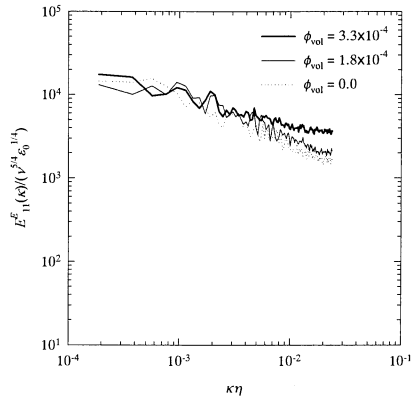

Figure 4. Profiles of streamwise velocity power spectra of water at the centerline of the channel in the presence of particles.

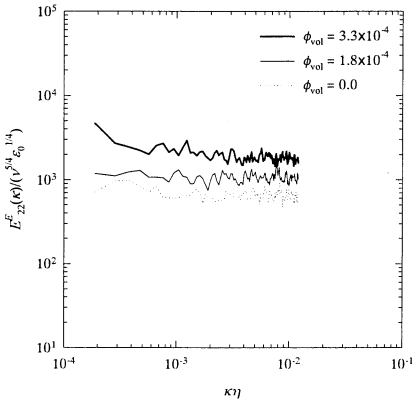

Figure 5. Profiles of transverse velocity power spectra of water at the centerline of the channel in the presence of particles.

$$\text{Gaussian}: G(x,y) = c_{G1}\exp\left[-\frac{6\left(x^2+y^2\right)}{\Delta^2}\right], \quad (2)$$

$$\text{top hat}: \quad G(x,y) = \begin{cases} c_{G2} \text{ if } |x| < \frac{1}{2}\Delta \text{ and } |y| < \frac{1}{2}\Delta \\ 0 \quad \text{otherwise} \end{cases}. \quad (3)$$

The coefficient c_G is a normalization factor which ensures that the integral of the filter equals unity (in the discrete sense).

Similarly, the SGS stress element, τ_{ij}, are computed to

$$\tau_{ij}(x,y) = \int_{-\infty}^{\infty}\int_{-\infty}^{\infty} U_{f_i}(x',y')U_{f_j}(x',y')G(x-x',y-y')\mathrm{d}x'\,\mathrm{d}y' - \tilde{u}_{f_i}(x,y)\tilde{u}_{f_j}(x,y) \quad (i=1,2). \quad (4)$$

The fields $\tilde{u}_{f_i}$ and τ_{ij} are frequently used as 'sampled' on a coarse mesh with a spacing of Δ.

A fluid flow is specified in the Eulerian way, while a Cartesian coordinate system is located on the high-speed CCD camera. The coordinate system moving with particle mean streamwise velocity is defined as both (x^C,y^C) and (x^C,z^C), where y^C and z^C are identical to y and z in the Eulerian reference frame, respectively. The fluctuating fluid velocity seen by particle is introduced as $u_f^{p>}$, where the superscript $p>$ stands for the turbulent property seen by particle

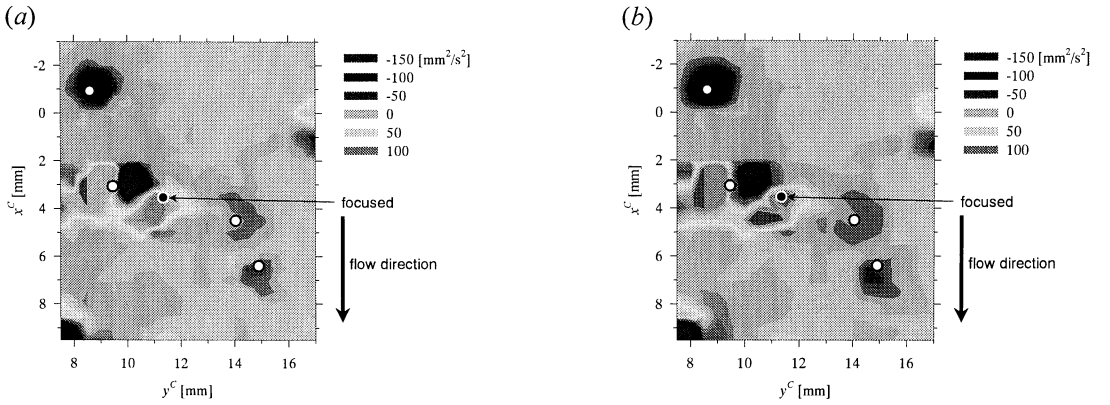

Figure 6. Contour plot of the real SGS stress element *seen by particle*, $\tau_{12}^{p>}$, computed with (*a*) the Gaussian filter of width Δ = 1 mm and (*b*) the top-hat filter of width Δ = 1mm. Fluid information *seen by particle* was calculated focusing on a particle as shown as a solid mark.

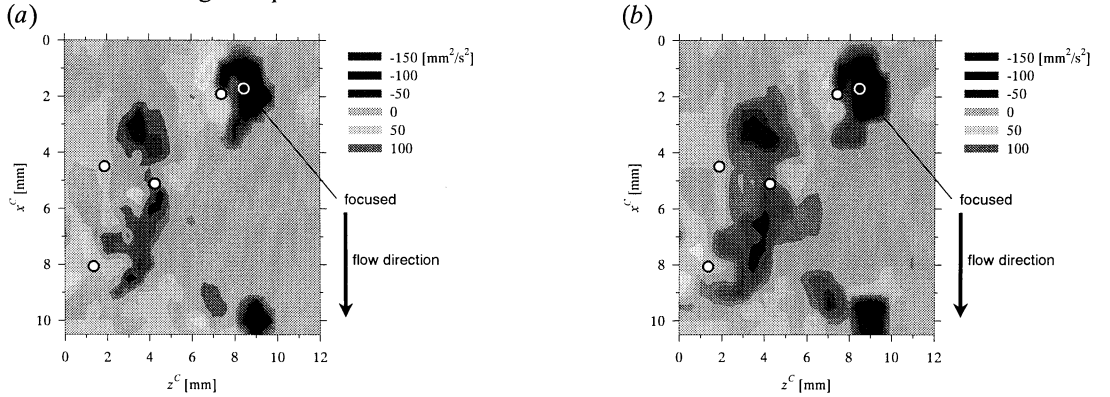

Figure 7. Contour plot of the real SGS stress element *seen by particle*, $\tau_{13}^{p>}$, computed with (*a*) the Gaussian filter of width Δ = 1 mm and (*b*) the top-hat filter of width Δ = 1mm. Fluid information *seen by particle* was calculated focusing on a particle as shown as a solid mark.

(Sato *et al.* 2000).

Figure 6 displays contour plots of the real SGS stress *seen by particle*, $\tau_{12}^{p>}$, computed with different filters. It is observed that both negative and positive values are appeared on both sides of the particle and there is no significant difference between the Gaussian and top-hat filters. Opposite trends are observed in *X-Z* plane. Figure 7 exhibits contour plots of the real SGS stress *seen by particle*, $\tau_{13}^{p>}$. Regions of negative values are dominant amongst particles and a slight effect of selection of filter on the real SGS stress was observed.

Energy flux to subgrid scales by particles

The total energy flux to unresolved scales *seen by particle* is defined as

$$\Pi(\Delta) = -\tau_{ij}^{p>}\tilde{S}_{ij}^{p>}, \qquad (5)$$

and one expects its (ensemble) average to be of the same order of magnitude as the dissipation rate, ε_{SGS}, in this near-equilibrium flow. Prior to investigation of energy transport by particles, the energy flux in each component was examined using the filtered fluid velocity *seen by particle*.

Figure 8 shows contour plot of the energy flux to SGS *seen by particle*, $-\tau_{12}^{p>}\tilde{S}_{12}^{p>}$, computed with different filters. It is obvious that regions of negative values are observed on both sides of particles, especially when particles was aligned with the transverse direction. The directional flow structure induced by particles was first reported by Sato *et al.* (2000), which was also found in the filtered velocity field. As the distance between particles, i.e., the inter-particle spacing (Crowe 1998, Crowe and Gillandt 1998, Sato *et al.* 2000), becomes narrower, the energy flux to SGS turns out to be negative, which means that the energy backscatter from SGS to grid scales (GS) is enhanced by particles.

Figure 9 displays contour plot of the energy flux to SGS *seen by particle*, $-\tau_{13}^{p>}\tilde{S}_{13}^{p>}$. Slight different trends are observed, however, regions of energy backscatter by particles was occurred when the inter-particle spacing becomes narrower.

One might imagine that one can see lots of particles more than the number displayed in the contour plots at high particle volumetric fraction, however, it is obvious from figures that there exist five or six glass particles in one image. In spite of *not-so-many* particles, fluid turbulence was significantly augmented in the presence of particles, because regions of energy backscatter by particles can be comparable to the size of energy-containing eddies, i.e., a few millimeters.

Energy dissipation and backscatter control by particles

The total energy flux to SGS and the SGS dissipation rate by particles are examined in this subsection in order to give further insight into the

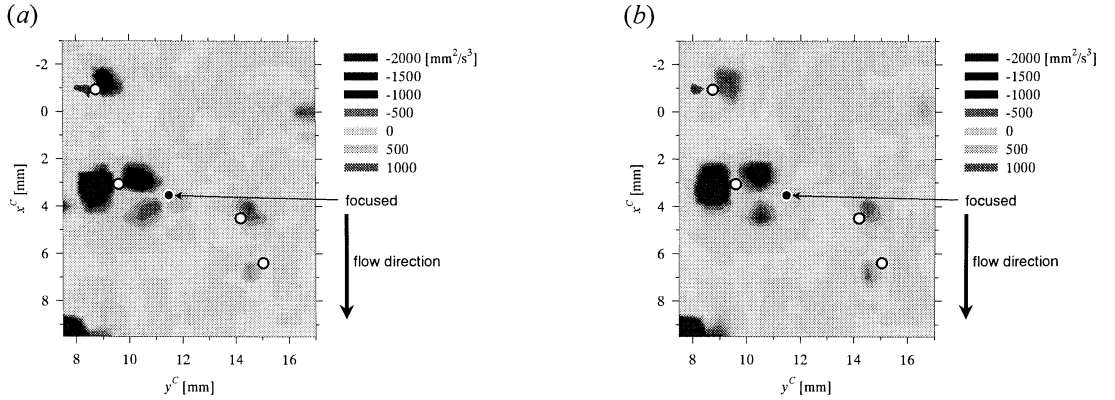

Figure 8. Contour plot of the energy flux to subgrid scale *seen by particle*, $-\tau_{12}^{p>}\bar{S}_{12}^{p>}$, computed with (*a*) the Gaussian filter of width Δ = 1 mm and (*b*) the top-hat filter of width Δ = 1mm. Fluid information *seen by particle* was calculated focusing on a particle as shown as a solid mark.

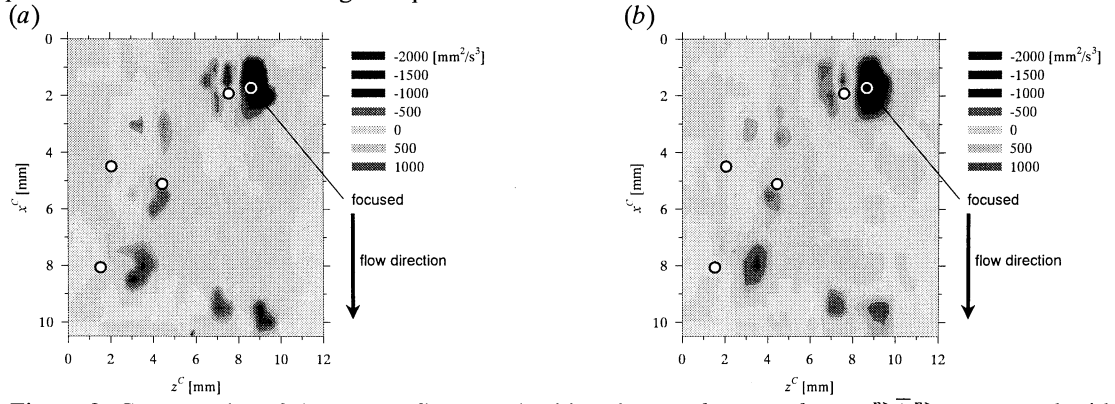

Figure 9. Contour plot of the energy flux to subgrid scale *seen by particle*, $-\tau_{13}^{p>}\bar{S}_{13}^{p>}$, computed with (*a*) the Gaussian filter of width Δ = 1 mm and (*b*) the top-hat filter of width Δ = 1mm. Fluid information *seen by particle* was calculated focusing on a particle as shown as a solid mark.

mechanism of energy transport by particles. The average value of energy flux, $\langle\Pi(\Delta)\rangle$, are calculated by averaging $\Pi(\Delta)$ using equation (5) in all the data set. Figure 10 shows the profiles of average SGS energy flux and energy backscatter control by particles as a function of the filter width Δ for the two filter types considered. The energy backscatter control by particles, $\varepsilon_{\text{backscatter}}$, is calculated by

$$\varepsilon_{\text{backscatter}} = \frac{1}{2}\left(\tau_{ij}^{p>}\tilde{S}_{ij}^{p>} + \left|\tau_{ij}^{p>}\tilde{S}_{ij}^{p>}\right|\right), \qquad (6)$$

where only the negative value of $\tau_{ij}^{p>}\tilde{S}_{ij}^{p>}$ is calculated in each image. It is obvious from figures 10(*a*) and 10(*b*) that an increase in particle volumetric fraction enhances the energy backscatter control by particles, however, this value is strongly dependent on the filter width for both filters. It can be seen that the effect of filter width on the average SGS energy flux is also significant, therefore a selection of filter width should be considered in modeling of SGS.

The SGS dissipation rate by particles is defined as

$$\varepsilon_{\text{SGS}} = \nu\overline{\frac{\partial u_{f_i}^{p>}}{\partial x_j}\frac{\partial u_{f_i}^{p>}}{\partial x_j}} - \frac{\partial \tilde{u}_{f_i}^{p>}}{\partial x_j}\frac{\partial \tilde{u}_{f_i}^{p>}}{\partial x_j}. \qquad (7)$$

Figure 11 exhibits profiles of the SGS energy dissipation as a function of filter width Δ for the two filter types considered. Higher the particle volumetric fraction becomes, larger the values of SGS dissipation rate is. It can be concluded that in the present experiments particles greater than the Kolmogorov micro length scale interact with fluid turbulence directionally, and enhance both the energy backscatter control and the SGS energy dissipation, yielding turbulence augmentation by particles.

CONCLUSIONS

A Lagrangian measurement technique has been used to investigate the energy transport by particles in a turbulent channel flow. The present study focused on the evolution of subgrid scale stresses in the presence of particles obtained from DPIV. The important conclusions obtained from this work are summarized below.

(1) A significant increase in turbulence energy in the transverse direction induces the directional interactions between fluid turbulence and particles.
(2) Distributions of the real SGS stresses *seen by particle* using filtered velocity field confirmed the directional non-isotropic structure of turbulence modification by particles.
(3) Particles which are greater than the Kolmogorov micro length scale enhance the energy backscatter especially when particles aligned with the transverse direction.
(4) An increase in particle volumetric fraction enhances the energy backscatter control by particles and the SGS dissipation by particles.

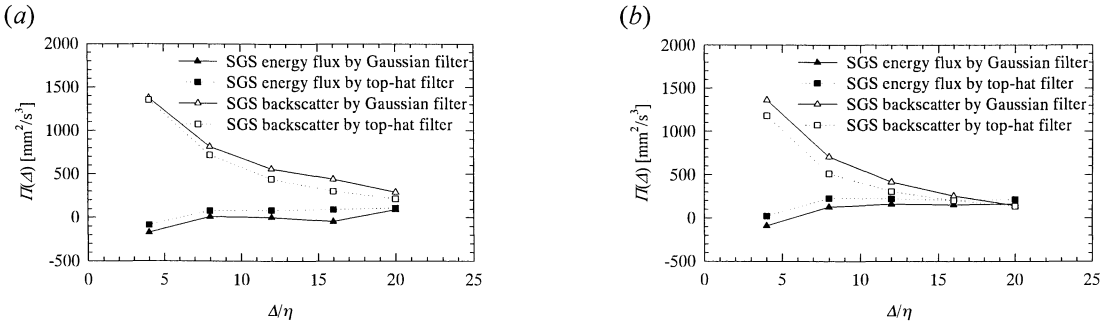

Figure 10. Profiles of average subgrid-scale energy flux and backscatter control in the presence of particles as function of filter size, Δ, at (*a*) $\phi_{vol} = 3.3\times10^{-4}$ and (*b*) $\phi_{vol} = 1.8\times10^{-4}$.

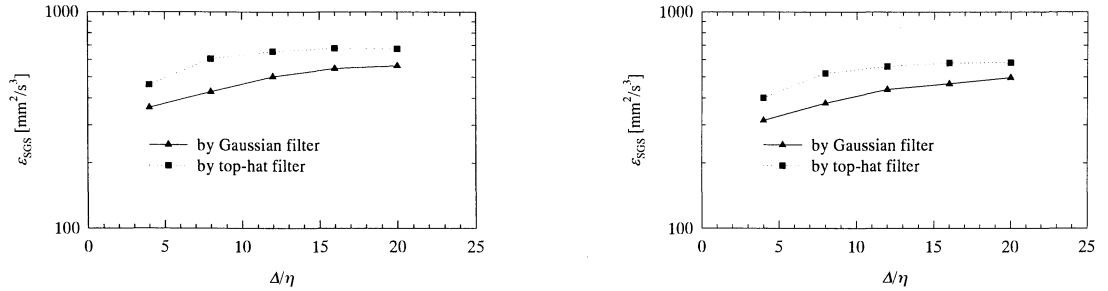

Figure 11. Profiles of energy dissipation in the presence of particles as function of filter size, Δ, at (*a*) $\phi_{vol} = 3.3\times10^{-4}$ and (*b*) $\phi_{vol} = 1.8\times10^{-4}$.

REFERENCES

Boivin, M., Simonin, O. and Squires, K.D., 1998, "Direct Numerical Simulation of Turbulence Modulation by Particles in Isotropic Turbulence," Journal of Fluid Mechanics, Vol. 375, pp. 235-263.

Crowe, C.T., 1998, "On Models for Turbulence in Fluid-Particle Flows," 1998 ASME Fluids Engineering Division Summer Meeting (CD-ROM).

Crowe, C.T., and Gillandt, I., 1998, "Turbulence Modulation of Fluid-Particle Flows – A Basic Approach," Third International Conference on Multiphase Flows (CD-ROM).

Eaton, J.K., 1994, "Experiments and Simulations on Turbulence Modification by Dispersed Particles," Applied Mechanics Review, Vol. 47, No. 6, Part 2, part of "Mechanics USA 1994" (A.S. Kobayashi ed.), S44-S48.

Elghobashi, S.E., and Truesdell, G.C., 1993, "On the Two-Way Interaction between Homogeneous Turbulence and Dispersed Solid Particles. I: Turbulence Modification," Physics of Fluids A, Vol. 5, pp. 1790-1801.

Fleckhaus, D., Hishida, K., and Maeda, M., 1987, "Effect of Laden Solid Particles on the Turbulent Flow Structure of a Round Free Jet," Experiments in Fluids, Vol. 5, pp. 323-333.

Gore, R.A., and Crowe, C.T., 1989a, "Effect of Particle Size on Modulating Turbulent Intensity," International Journal of Multiphase Flow, Vol. 15, pp. 279-285.

Gore, R.A., and Crowe, C.T., 1989b, "Effect of Particle Size on Modulating Turbulent Intensity: Influence of Radial Location," Turbulence Modification in Dispersed Multiphase Flow, ASME-FED, Vol. 80, pp. 31-35.

Hishida, K., and Sato, Y., 1999, "Turbulence Structure of Dispersed Two-Phase Flows (Measurements by Laser Techniques and Modeling)," Multiphase Science and Technology, Vol. 10, pp. 323-346.

Kulick, J.D., Fessler, J.R., and Eaton, J.K., 1994, "Particle Response and Turbulence Modification in Fully Developed Channel Flow," Journal of Fluid Mechanics, Vol. 277, pp. 109-134.

Rogers, C.B., and Eaton, J.K., 1991, "The Effect of Small Particles on Fluid Turbulence in a Flat-Plate, Turbulent Boundary Layer in Air," Physics of Fluids A, Vol. 3, pp. 928-937.

Sakakibara, J., Hishida, K., and Maeda, M., 1993, "Measurements of Thermally Stratified Pipe Flow Using Image-processing Techniques," Experiments in Fluids, Vol. 16, pp. 82-96.

Sato, Y., Fukuichi, U., and Hishida, K., 2000, "Effect of Inter-Particle Spacing on Turbulence Modulation by Lagrangian PIV," International Journal of Heat and Fluid Flow, Vol. 21, pp. 554-561.

Sato, Y., Hayashi, I., and Hishida, K., 1997, "Lagrangian Statistics of Fluid/Particle Correlated Motion in Channel Flow," Eleventh Symposium on Turbulent Shear Flows, Vol. 3, pp. 24-11 – 24-16.

Sato, Y., and Hishida, K., 1996, "Transport Process of Turbulence Energy in Particle-Laden Turbulent Flow," International Journal of Heat and Fluid Flow, Vol. 17, pp. 202-210.

Squires, K.D., and Eaton, J.K., 1990, "Particle Response and Turbulence Modification in Isotropic Turbulence," Physics of Fluids A, Vol. 2, pp. 1191-1203.

Tsuji, Y., and Morikawa, Y., 1982, "LDV Measurements of an Air-Solid Two-Phase Flow in a Horizontal Pipe," Journal of Fluid Mechanics, Vol. 120, pp. 385-409.

Tsuji, Y., Morikawa, Y., and Shiomi, H., 1984, "LDV Measurements of an Air-Solid Two-Phase Flow in a Vertical Pipe," Journal of Fluid Mechanics, Vol. 139, pp. 417-434.